

Article

Enhancing Chatter Stability for Milling Thin-Walled Blades by Designing Non-Uniform Allowance

Yu Li ^{1,2}, Feng Ding ^{1,*}, Weijun Tian ³ and Jinhua Zhou ^{4,*} ¹ School of Mechatronic Engineering, Xi'an Technological University, Xi'an 710021, China; liyuu@mdit.edu.cn² School of Intelligent Manufacturing and Control Technology, Xi'an MingDe Institute of Technology, Xi'an 710124, China³ Engineering Practice Training Center, Northwestern Polytechnical University, Xi'an 710129, China; tianwj@nwpu.edu.cn⁴ School of Mechanical Engineering, Northwestern Polytechnical University, Xi'an 710072, China

* Correspondence: dfeng@xatu.edu.cn (F.D.); zhoujinhua@mail.nwpu.edu.cn (J.Z.)

Abstract: During the milling of thin-walled blades, the removal of material exhibits strong time-varying dynamics, leading to chatter and a decrease in surface quality. To address the issue of milling vibrations in the machining of complex thin-walled blades used in aerospace applications, this work proposes a process optimization approach involving non-uniform allowances. The objective is to enhance the stiffness of the thin-walled parts during the milling process by establishing a non-uniform allowance distribution for the finishing process of thin-walled blades. By applying the theory of sensitive process stiffness and conducting finite element simulations, two processing strategies, namely uniform allowances and non-uniform allowances, are evaluated through cutting experiments. The experimental results demonstrate that the non-uniform allowance processing strategy leads to a more evenly distributed acceleration spectrum and a 50% reduction in amplitude. Moreover, the surface exhibits no discernible vibration pattern, resulting in a 35% decrease in roughness. The non-uniform allowance-processing strategy proves to be effective in significantly improving the rigidity of the thin-walled blade processing system, thereby enhancing the stability of the cutting process. These findings hold significant relevance in guiding the machining of typical complex thin-walled aerospace components.

Keywords: thin-walled parts; vibration; sensitivity; stiffness; allowance

Citation: Li, Y.; Ding, F.; Tian, W.; Zhou, J. Enhancing Chatter Stability for Milling Thin-Walled Blades by Designing Non-Uniform Allowance. *Appl. Sci.* **2023**, *13*, 13340. <https://doi.org/10.3390/app132413340>

Received: 20 October 2023

Revised: 5 December 2023

Accepted: 13 December 2023

Published: 18 December 2023



Copyright: © 2023 by the authors. Licensee MDPI, Basel, Switzerland. This article is an open access article distributed under the terms and conditions of the Creative Commons Attribution (CC BY) license (<https://creativecommons.org/licenses/by/4.0/>).

1. Introduction

Blades, constituting approximately 30% of the manufacturing process of an aircraft engine, are an essential component with regard to its performance [1–5]. Consequently, CNC precision machining technology has become the primary method for manufacturing blades worldwide. However, during the milling process of a thin-walled blade, its overhang gradually increases as the wall thickness is reduced. The dynamic characteristics of the blade, with changes in cutting position and material removal, display a strong time-varying nature. This feature can easily lead to the chatter phenomenon during milling, resulting in a decline in machining surface quality and accuracy, which can significantly impact on the blade's performance [6–10]. Chattering during the milling process of thin-walled blades remains to be a significant technical challenge within the aero-engine manufacturing industry.

In recent years, researchers from domestic and international institutions have undertaken comprehensive investigations into the milling vibration problem related to thin-walled blades. The focus of these studies has primarily revolved around analyzing the dynamics of the milling process system model and employing the Floquet theory to establish stability criteria. The thin-walled cutting modal parameter, which is susceptible to varying conditions over time, has been taken into account to predict process system

stability with ultimate depth of cut and speed. This has contributed to stability lobe formation. For instance, Hamann et al. combines parametric model downscaling of time-lagged systems with stability analysis to improve computational simulation efficiency, predicting the stability domain while considering the influence of material removal on processing system dynamics [11]. Wan and other scholars developed an effective method for predicting stability lobes in multimodal milling systems across all main chirp modes in the time domain [12–15]. Recently, some scholars employed random variables to set the structural parameters of the milling processing system and spindle speed while using chattering frequency as an intermediate variable. These measures help establish a reliability model for locating the probability of side milling stability. This model replaces the traditional stability leaflet prediction diagram with a more accurate method [16–18]. For instance, Huang et al. presents a useful probabilistic forecast approach to estimate the dynamic stability during the milling process. This method takes into consideration the uncertain system parameters of the milling process [19]. In addition, Hu employs neural networks to carry out an extensive analysis of the influence of random factors in milling processing. Subsequently, he proposes a probabilistic assessment technique to predict the reliability of regenerative chattering stability during milling [20]. Zhang et al. considers the influence of random variables on the stability of overall blisk side milling machining to accurately predict the value [21]. By applying the reliability analytic approach to the dynamic structural system, a chatter reliability model for the side milling machining system of an overall blisk is established. Those previous researchers have commonly started by developing a dynamic model of the process system, obtaining its structural parameters, and adjusting the process parameters to achieve cutting stability. The accuracy of extracting process parameters and the influence of external factors significantly affect the predictive capability of the system.

In light of chatter active control, adding an active controller to the milling process system reduces the chatter problem of the system. For instance, Li et al. suggests a robust controller based on linear matrix inequalities to model the chatter active control system for milling, and the results evidences significant enhancement in the milling surface finish and the chatter-free boundary [22]. Lee et al. proposes an active control technique to decrease milling vibration by utilizing a voice coil motor and a laser displacement detector as actuator and sensor, whose results demonstrate the feasibility and superiority of the proposed technique as well as the closed-loop system [23]. Moreover, Du et al. proposes an active control method using piezoelectric patch actuators to enhance the stability of the milling process [24]. These scholars approach chatter suppression from the perspective of active control, who design the actuator installed in the spindle system based on the working conditions. Though somehow cumbersome, this implementation is more effective in reducing tool chatter. However, the suppression effect is still limited to thin-walled parts. Furthermore, to enhance cutting stability, one can alter the milling cutter's structural parameters by adjusting its helix angle and tooth pitch distribution. For instance, Buransky et al. examines the impact of variable pitch on end milling cutters for surface quality and flatness. The findings demonstrate that an irregular pitch end milling cutter can decrease chatter when milling thin-walled parts and simultaneously increase cutting speed [25]. Tehranizadeh et al. conducted an analysis and comparison of the standard, variable-pitch and wave cutters for suppressing chatter in thin-walled milling, whose experiment results demonstrated that the wave cutter has a certain degree of advantage in chatter suppression for thin-walled machining and this cutter can effectively reduce chatter in thin-walled machining [26]. Zheng et al. creates a cutting force model for variable-pitch end mills and confirms the link between material removal and vibration response using the optimal inter-tooth angle [27]. Guo et al. devises a non-uniform helical tool dynamics equation and suggests cutting stability limitations. The dependability of the forecast model was authenticated through experiments [28]. Jiang et al. establishes a model for demonstrating the dynamic and stability aspects of variable pitch/helix angle milling that takes into account tool runout. He proposes an updated cross-axis and cross-point modal testing method to obtain dynamic parameters that can effectively circumvent vibration issues [29].

The researchers mentioned above focus primarily on the non-uniform side milling of flat-bottomed milling cutters; however, there are limited studies on the milling of thin-walled parts with ball-ended cutters. Wu et al. proposed an optimization method of machining process with non-uniform allowance of integral impeller to accurately improve and predict chatter stability region of machining process [30]. Tian et al. determined and optimized the allowance distribution state of simple thin-walled workpiece in semi-finishing machining based on eigenvalue sensitivity analysis method [31]. However, for complex thin-walled blade structures, the improvement of machining stability through non-uniform margin design still deserves further in-depth research.

There are also methods available for the milling process system to absorb and damp vibrations by modifying the system damping mode. For instance, Jiang et al. devises a kinetic model for MRF clamping grounded on fuel-solid coupling kinetic theory and puts forth an MRF composite fixture to diminish milling vibration [32]. Yuan et al. suggests a method for suppressing forced vibration in thin-walled workpieces, where STF can effectively suppress the forced vibration effect during the milling process [33]. Dang et al. proposes a theoretical methodology to analyze the dynamic behavior of the thin-walled workpiece milling process filled with a viscous fluid to suppress chattering. Optimal process parameters have been achieved through a dynamic model of the spindle-tool system and a thin-walled workpiece immersed in a viscous fluid [34]. Zhang et al. developed a novel technique to attenuate chattering vibration of a thin-walled workpiece by immersing the milling system in a viscous fluid. The findings demonstrate that the technique expertly suppresses the chattering of thin-walled workpieces and attains a high stability limit [35]. Ultimately, the procedure for adjusting the process stiffness of thin-walled components is achieved by applying the method with non-uniform allowances [36–39]. Built upon the above studies, this thesis centers around how the traditional design of thin-walled parts can produce a certain inhibitory effect. While examining current research, it is found that there is limited studies on the inhibitory effects of complex thin-walled structural parts, and the current distribution method remains relatively inaccurate.

From the literature reviewed, it is evident that several studies have focused on enhancing the machining stability of those regular thin-walled components. However, the machining stability of such complex aerospace blades deserves further in-depth study, especially through the non-uniform allowance design to improve the machining stability. Built upon the sensitivity process stiffness enhancement theory, a more accurate method optimized for non-uniform allowance process in the milling process of thin-walled parts is proposed herein. In the following analysis, Section 2 focuses on analyzing the effect of allowances distribution on the dynamic characteristics of thin-walled parts blade, and then presents the optimal design theory to address stiffness in light of the sensitivity theory. On the basis of the idea of finite element combined with the optimal design theory, it further seeks for a non-uniform allowance distribution design for the blade. Section 3 starts with an example of the typical blade to carry out design and experimental verification of the non-uniform allowance distribution. Results prove that the non-uniform allowance design based on sensitivity design proposed herein is effective to achieve stability during the milling process of blades of typical thin-walled parts used in aviation.

2. Description of the Methodology

2.1. Analysis of the Effect of Allowances Distribution on Blade Dynamic Characteristics

The blade's complex structure is designed according to its own dynamic characteristics. The leading and trailing allowances incorporate a rounded surface transition that is very thin while the blade body comprises transverse cross-sections that vary across its surface. Its body surface consists of a base surface and a tongue-and-groove root surface cropping. The axial stack of the blade accumulates with a certain degree of torsion. To effectively present the proposed optimal design method while ensuring its applicability and facilitating meshing and finite element analysis, a simplification technique has been employed. Through the utilization of hexahedral cells, the blade has been simplified with utmost

precision, minimizing any distortion that may compromise its integrity, as illustrated in Figure 1.

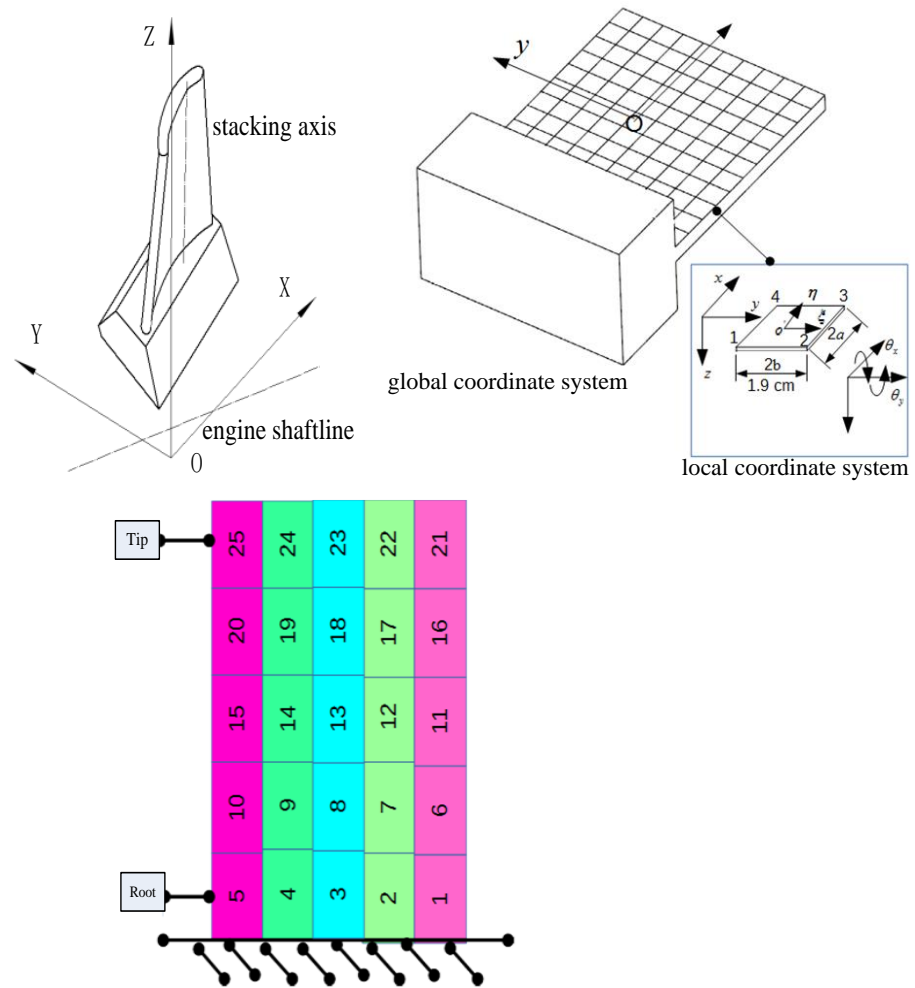


Figure 1. Grid cell division.

Based on the finite element method, the physical blade is simplified and discretized into a continuum structure as illustrated in Figure 1. The control equations for the resulting multi-degree-of-freedom dynamical system can thus be formulated as shown bellow.

$$[M]\{\ddot{x}(t)\} + [C]\{\dot{x}(t)\} + [K]\{x(t)\} = [f(t)] \tag{1}$$

where the matrices $[M]$, $[C]$, and $[K]$, respectively, denote the mesh mass, damping, and stiffness distributions of the discretized blade. The vector distributions $\{\ddot{x}(t)\}$, $\{\dot{x}(t)\}$, and $\{x(t)\}$, respectively, denote the mesh node acceleration, velocity, and displacement. Proportional damping can be assumed in this case.

$$[C] = \alpha[M] + \beta[K] \tag{2}$$

where α and β are constants of proportionality and Equation (1) is transformed modally.

$$\{x(t)\} = \sum_{r=1}^N q_r \{\phi_r\} \tag{3}$$

$$\{\phi_r\}^T [C] \{\phi_r\} = \alpha \{\phi_s\}^T [M] \{\phi_r\} + \beta \{\phi_s\}^T [K] \{\phi_r\} = \begin{cases} 0 & r \neq s \\ \alpha m_s + \beta k_s = c_s, & r = s \end{cases} \tag{4}$$

In Equation(4) $\{\phi_r\}$ is the r th order mode shape determined by $[M]\{\ddot{x}(t)\} + [K]\{x(t)\}$ and q_r is the corresponding mode coordinate obtained by substituting Equation (3) into Equation (1).

$$[M]\left(\sum_{r=1}^N \ddot{q}_r\{\phi_r\}\right) + [C]\left(\sum_{r=1}^N \dot{q}_r\{\phi_r\}\right) + [K]\left(\sum_{r=1}^N q_r\{\phi_r\}\right) = \{f(t)\} \tag{5}$$

The above equation is left multiplied by $\{\phi_r\}^T$, according to the assumed damping. Then, the above equation can be expressed as follows:

$$m_s \ddot{q}_s + c_s \dot{q}_s + k_s q_s = \{\phi_s\}^T \{f(t)\} \tag{6}$$

If $\{f(t)\} = \{F\}e^{j\omega t}$ is given, then by substituting $q_s = Q_s e^{j\omega t}$ into Equation (6), one can obtain Equation (7) as follows:

$$\left(-\omega^2 m_s + j\omega c_s + k_s\right) Q_s e^{j\omega t} = \{\phi_s\}^T \{F\} e^{j\omega t} \tag{7}$$

From this one can derive Equation (8) as follows:

$$Q_s = \frac{\{\phi_s\}^T \{F\}}{-\omega^2 m_s + j\omega c_s + k_s} \propto y = \frac{f}{k} \tag{8}$$

From the above equation, it is clear that Q_s corresponds to the displacement response resulting from a single-degree-of-freedom system, which includes masses, damping, and stiffnesses m_s , c_s and k_s , respectively, when under the action of the modal force $P_s = \{\phi_s\}^T \{F\}$. Meanwhile, $(-\omega^2 m_s + j\omega c_s + k_s)$ represents the stiffness of the system and is referred to as the dynamic stiffness.

$$\{x\} = \begin{Bmatrix} X_1 \\ X_2 \\ \vdots \\ X_N \end{Bmatrix} e^{j\omega t} = \sum_{r=1}^N q_r \{\phi_r\} = \sum_{r=1}^N Q_r \{\phi_r\} e^{j\omega t} \tag{9}$$

Through the above derivation, it becomes clear that altering the mass distribution of the grid cells on the blade results in a change in the dynamic stiffness $(-\omega^2 m_s + j\omega c_s + k_s)$, leading to variations in the dynamic characteristics. Essentially, the mass distribution of the cells will impact the overall stiffness of the blade.

In order to mitigate any potential errors in optimizing the structural dynamic characteristics, it is imperative to conduct a comprehensive sensitivity analysis on the design parameters using advanced optimization analysis techniques. This entails accurately assessing the impact of each individual design variable on the dynamic performance of the process system, which subsequently aids in optimizing the distribution of allowances. To accomplish this, the dynamic eigenvalue sensitivity approach is employed as a vital tool for optimizing the allowances distribution. By leveraging the insights gained from this sensitivity analysis, an informed and effective optimization strategy can be implemented to refine the distribution of allowances, ensuring optimal dynamic performance of the system.

2.2. First-Order Sensitivity Calculation for Thin-Walled Blades

Since the distribution of allowances across the blade has the most significant effect on the first order modal frequencies of the blade, the allowance distribution can be optimized by selecting the sensitivity of the eigenvalues of the blade to change in the mass distribution and stiffness of the mesh. The sensitivity can be defined as the rate of change of the index

of interest in response to specific structural parameters. Mathematically, this is expressed as the first-order derivative of a derivable function.

$$S = (F)_j = \frac{\partial F(x)}{\partial x_j} \tag{10}$$

For structural vibration systems, dynamic response sensitivity can be understood as the rate of change of the response parameters (eigenvalues λ and eigenvectors φ) with respect to the structural parameters (or other design variables), that is eigenvalue sensitivity $\partial\lambda/\partial p_m$ and eigenvector sensitivity $\partial\varphi/\partial p_m$, where p_m are structural parameters (including mass, stiffness, and damping) or design variables. For a viscous damped system with N degrees of freedom, the degree of freedom vibration equation of motion can be expressed as follows:

$$M\ddot{X} + C\dot{X} + KX = 0 \tag{11}$$

where M, K, C represent the mass, stiffness and damping matrices of the structure, M a positive definite matrix, K and C the non-negative definite matrices while X the displacement response column vector as in $X^T = [x_1(i), x_2(i), x_3(i) \dots x_N(i)]$.

Let the state vector be as follows:

$$X = \left\{ \begin{matrix} X \\ \dot{X} \end{matrix} \right\}_{2N \times 1} \tag{12}$$

It follows that as follows:

$$A\dot{X} + BX = 0 \tag{13}$$

where $A = \begin{bmatrix} C & M \\ M & 0 \end{bmatrix}; B = \begin{bmatrix} K & 0 \\ 0 & -M \end{bmatrix}$ The characteristic equation of Equation (13) has a complex conjugate characteristic pair, i.e., $\lambda_r, \bar{\psi}_r, \lambda_r^*, \bar{\psi}_r^*$ ($r = 1, 2, \dots, N$)

It can be obtained for the modes of the r th order.

$$\lambda A\bar{\psi}_r + B\bar{\psi}_r^* = 0 \tag{14}$$

where $\bar{\psi}_r = \left\{ \begin{matrix} \psi_r \\ \lambda_r \psi_r \end{matrix} \right\}, \bar{\psi}_r^* = \left\{ \begin{matrix} \psi_r^* \\ \lambda_r^* \psi_r^* \end{matrix} \right\}$.

It is obtained from the orthogonality condition of the modal vector as follows:

$$\bar{\psi}_r^T A \bar{\psi}_s = a_r \delta_r \tag{15}$$

$$\bar{\psi}_r^T B \bar{\psi}_s = b_r \delta_r \tag{16}$$

where δ_r is the Kronecker delta function when $r \neq s, \delta_r = 0$, and when $r = s, \delta_r = 1$. The weighting is applied to $\bar{\psi}_r$, such that

$$\bar{\psi}_r = \bar{\psi}_r / \sqrt{a_r} = \left\{ \begin{matrix} \tilde{\psi}_r \\ \lambda_r \tilde{\psi}_r \end{matrix} \right\}, \bar{\psi}_r^T = [\varphi_1, \varphi_2, \dots, \varphi_N]_r$$

Then, Equations (15) and (16) can be written as follows:

$$\bar{\psi}_r^T A \bar{\psi}_r = I \tag{17}$$

$$\bar{\psi}_r^T B \bar{\psi}_r = -\lambda_r \tag{18}$$

So, for complex modes, we use the following:

$$\lambda_r A \bar{\psi}_r + B \bar{\psi}_r = 0 \tag{19}$$

$$\lambda_r \bar{\psi}_r^T A \bar{\psi}_r + \bar{\psi}_r^T B \bar{\psi}_r = 0 \tag{20}$$

$$\lambda_r \bar{\psi}_r^T A + \bar{\psi}_r^T B = 0 \tag{21}$$

An expression for the sensitivity of the characteristic curve can be derived from the above equation. If the structural parameter p_m is a derivative of Equation (19), then one can have

$$\frac{\partial \lambda_r}{\partial p_m} A \bar{\psi}_r + \lambda_r \frac{\partial A}{\partial p_m} \bar{\psi}_r + \lambda_r A \frac{\partial \bar{\psi}_r}{\partial p_m} + \frac{\partial B}{\partial p_m} \bar{\psi}_r + B \frac{\partial \bar{\psi}_r}{\partial p_m} = 0 \tag{22}$$

Multiplication $\bar{\psi}_r^T$ of the above equation by A on the left gives

$$\frac{\partial \lambda_r}{\partial p_m} \bar{\psi}_r^T A \bar{\psi}_r + \lambda_r \bar{\psi}_r^T \frac{\partial A}{\partial p_m} \bar{\psi}_r + \bar{\psi}_r^T \frac{\partial B}{\partial p_m} \bar{\psi}_r + (\lambda_r \bar{\psi}_r^T A + \bar{\psi}_r^T B) \frac{\partial \bar{\psi}_r}{\partial p_m} = 0 \tag{23}$$

It can be obtained from Equations (17) and (21).

$$\frac{\partial \lambda_r}{\partial p_m} = -\lambda_r \bar{\psi}_r^T \frac{\partial A}{\partial p_m} \bar{\psi}_r - \bar{\psi}_r^T \frac{\partial B}{\partial p_m} \bar{\psi}_r \tag{24}$$

The above equation can be further extended as follows:

$$\frac{\partial \lambda_r}{\partial p_m} = -(\lambda_r^2 \psi_r^T \frac{\partial M}{\partial p_m} \psi_r + \lambda_r \psi_r^T \frac{\partial C}{\partial p_m} \psi_r + \psi_r^T \frac{\partial K}{\partial p_m} \psi_r) \tag{25}$$

where ψ_r is the upper half vector of $\bar{\psi}_r$ and M, C and K the mass, damping and stiffness matrices of order $N \times N$. This gives an expression for the first order eigenvalue sensitivity.

(1) Sensitivity of eigenvalues to m_{ij}

$$\frac{\partial \lambda_r}{\partial m_{ij}} = -\lambda_r^2 \psi_r^T \frac{\partial M}{\partial m_{ij}} \psi_r \tag{26}$$

Since M is a symmetric matrix, it can be deduced as follows:

$$\frac{\partial \lambda_r}{\partial m_{ij}} = \begin{cases} -2\lambda_r^2 \varphi_{ir} \varphi_{jr}, & (i \neq j) \\ -\lambda_r^2 \varphi_{ir}^2, & (i = j) \end{cases} \tag{27}$$

(2) Sensitivity of eigenvalues to k_{ij}

$$\frac{\partial \lambda_r}{\partial k_{ij}} = -\psi_r^T \frac{\partial K}{\partial k_{ij}} \psi_r \tag{28}$$

It can be further deduced as follows:

$$\frac{\partial \lambda_r}{\partial k_{ij}} = \begin{cases} -2\varphi_{ir} \varphi_{jr}, & (i \neq j) \\ -\varphi_{ir}^2, & (i = j) \end{cases} \tag{29}$$

Upon obtaining the sensitivity of the process system eigenvalues with respect to stiffness, the sensitivity at the blade’s central axis position serves as a critical reference for further analysis. By adjusting the thickness of the grid cells on either side in a rational manner, the sensitivity of the blade’s grid cells can be effectively homogenized, ensuring that the process of milling the material results in consistent stiffness removal trends. The adjustment amount Δ_i of the thickness of the mesh nodes indirectly reflects the geometric distribution of the spatial nodes of the non-uniform allowances at each cross-section position.

2.3. Design of Thin-Walled Blade Allowance Distribution Based on First-Order Sensitivity

Suppose eigenvalues λ and eigenvectors ψ_r are multivariate functions of structural parameters m_{ij}, k_{ij} , and c_{ij} .

$$(\lambda_r, \psi_r) = f(m_{ij}, k_{ij}, c_{ij}) \tag{30}$$

where m_{ij} , k_{ij} and c_{ij} are the i -th row and j -th column elements of the mass matrix M , stiffness matrix K and damping matrix C equations, respectively. The above equation can be expanded into a Taylor series.

$$\begin{aligned} \lambda_r &= \bar{\lambda}_r + \Delta\lambda_r = \bar{\lambda}_r + \sum_{i=1}^N \sum_{j=1}^N \left(\frac{\partial\lambda_r}{\partial m_{ij}}\right)\Delta m_{ij} + \sum_{i=1}^N \sum_{j=1}^N \left(\frac{\partial\lambda_r}{\partial k_{ij}}\right)\Delta k_{ij} + \sum_{i=1}^N \sum_{j=1}^N \left(\frac{\partial\lambda_r}{\partial c_{ij}}\right)\Delta c_{ij} \\ &+ \frac{1}{2!} \sum_{i=1}^N \sum_{j=1}^N \left(\frac{\partial^2\lambda_r}{\partial m_{ij}^2}\right)\Delta m_{ij}^2 + \frac{1}{2!} \sum_{i=1}^N \sum_{j=1}^N \left(\frac{\partial^2\lambda_r}{\partial k_{ij}^2}\right)\Delta k_{ij}^2 + \frac{1}{2!} \sum_{i=1}^N \sum_{j=1}^N \left(\frac{\partial^2\lambda_r}{\partial c_{ij}^2}\right)\Delta c_{ij}^2 \\ &\frac{1}{2!} \sum_{i=1}^N \sum_{j=1}^N \sum_{p=1}^N \sum_{q=1}^N \left(\frac{\partial^2\lambda_r}{\partial m_{ij}k_{pq}}\right)\Delta m_{ij}\Delta k_{pq} + \frac{1}{2!} \sum_{i=1}^N \sum_{j=1}^N \sum_{p=1}^N \sum_{q=1}^N \left(\frac{\partial^2\lambda_r}{\partial m_{ij}c_{pq}}\right)\Delta m_{ij}\Delta c_{pq} \\ &\frac{1}{2!} \sum_{i=1}^N \sum_{j=1}^N \sum_{p=1}^N \sum_{q=1}^N \left(\frac{\partial^2\lambda_r}{\partial k_{ij}c_{pq}}\right)\Delta k_{ij}\Delta c_{pq} \end{aligned} \tag{31}$$

In the actual calculation, due to the finishing process of thin-walled parts, the correction amount of structural parameters is very small. Therefore, the second-order correction term can be ignored, and the eigenvalue correction amount is as follows:

$$\Delta\lambda_r = \sum_{i=1}^N \sum_{j=1}^N \left(\frac{\partial\lambda_r}{\partial m_{ij}}\right)\Delta m_{ij} + \sum_{i=1}^N \sum_{j=1}^N \left(\frac{\partial\lambda_r}{\partial k_{ij}}\right)\Delta k_{ij} + \sum_{i=1}^N \sum_{j=1}^N \left(\frac{\partial\lambda_r}{\partial c_{ij}}\right)\Delta c_{ij} \tag{32}$$

The derivatives in the equation are calculated for the initial eigenvalue $\bar{\lambda}_r$ and eigenvector $\bar{\psi}_r$. Via the above analysis, the sensitivity can be obtained given the condition of neglected damping. The correction Δm_{ij} can be determined by evaluating the change in $\Delta\lambda_r$ and $\Delta\psi_r$, and the change in Δk_{ij} results from each individual mass change.

$$\Delta m_{ij} = \frac{1}{\sum_{i=1}^N \sum_{j=1}^N \left(\frac{\partial\lambda_r}{\partial m_{ij}}\right)} \left(\Delta\lambda_r - \sum_{i=1}^N \sum_{j=1}^N \left(\frac{\partial\lambda_r}{\partial k_{ij}}\right)\Delta k_{ij} \right) \tag{33}$$

Once the change in the grid cell mass is determined, the corresponding change Δh_{ij} in height along the Z-axis can be ascertained using the geometric relationship as hexahedral grid cells are utilized.

$$\Delta h_{ij} = h_{ij} - \frac{\Delta m_{ij}}{\rho \cdot S} \tag{34}$$

The calculation using Matlab-based Equation (34) allows for obtaining the height change amount of all grid cells at the same level of stiffness. To achieve smooth non-uniform bias surfaces, it is possible to consider interpolation between grid nodes, as in Equation (35) to obtain the final cross-section bias curve.

$$S_k(x) = y_k\alpha_0^{(k)}(x) + y_{k+1}\alpha_1^{(k)}(x) + m_k\beta_0^{(k)}(x) + m_{k+1}\beta_1^{(k)}(x) \tag{35}$$

Through analogy, one can determine the thickness of a unit node within a cross-section of a thin-walled blade. Subsequently, the cross-section curves can be deduced using interpolation, leading to the acquisition of a bias mesh surface with non-uniform thickness for the entire blade via interpolation of each cross-section curve.

3. Example Analysis: Designing Non-Uniform Allowance for Milling Thin-Walled Blades of Titanium Alloy TC4

The blade has an inlet spread length of 64.7 mm and an exhaust side spread length of 55.0 mm. The tip chord measures 41.3 mm, with the thinnest and thickest points at 0.34 mm and 1.1 mm, respectively. At the root, the blade has the thinnest point of 1.6 mm and the thickest point of 4.11 mm with a root fillet radius of 2.5 mm. The figure in Figure 2 displays the experimental blade made of TC4 titanium alloy with solid structural features. The variable cross-section twisted free-form surface of the blade requires corresponding design allowances for finishing.

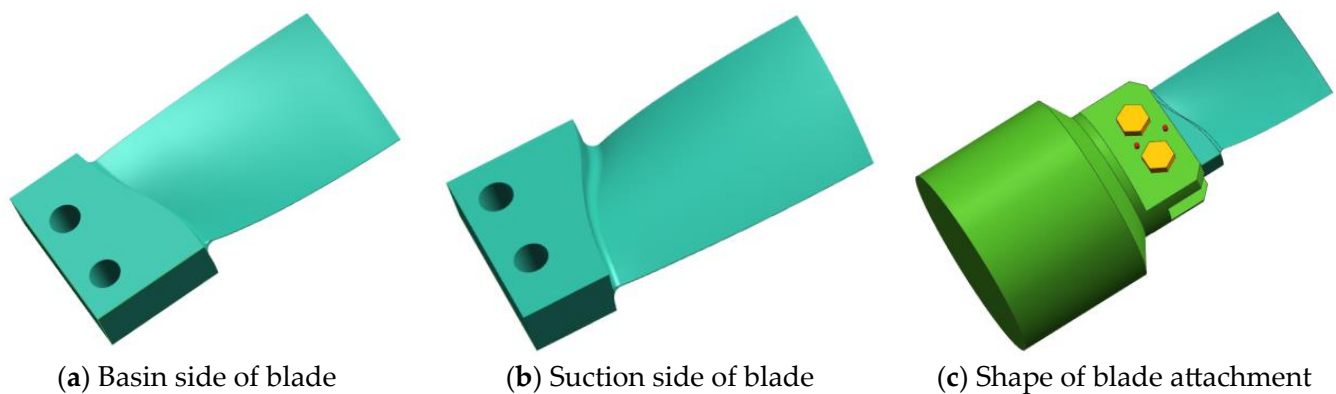


Figure 2. Schematic diagram of blade structure.

Design basic processes and steps is as follows.

- (1) The process system is first meshed, and the mass and stiffness matrices are calculated according to reference [1].
- (2) Sensitivity calculation of eigenvalue to mass (Equation (27)) and stiffness (Equation (29)) in the first order.
- (3) Calculation of the correction (Equation (33)) with reference to the sensitivity of blade mid-axis position.
- (4) Generation of mesh node interpolation heights (Equations (33) and (34)).
- (5) Creating the blade cross-section curve using the nodes to form a non-uniform allowances mesh bias surface.
- (6) Using the bias surface as the driving surface for CNC finishing programming.

3.1. Calculation of First-Order Sensitivity of Eigenvalues of Thin-Walled Blades

Using the method outlined in Section 2.2 for calculating the first-order sensitivity of thin-walled blades while referring to the literature [1], the overall stiffness matrix (K) and mass matrix (M) of the thin-walled blade surface are computed through programming in the Matlab environment. Upon substitution into Equations (27) and (29), the eigenvalue-to-stiffness sensitivity depicted in Figure 3 and the eigenvalue-to-mass sensitivity shown in Figure 4 are obtained through programming calculations, respectively. The x - y axes in the horizontal plane represent the grid node divisions and the vertical plane axis z represents the sensitivity amplitude. Technical abbreviations are defined upon their first use.

Based on the calculation results, it is telling that thin-walled blades possess a consistent trend in terms of their characteristics for mass sensitivity and stiffness sensitivity. The overall performance of the blade is concentrated on both sides of the allowances, with the main sensitive area being the tip. Moreover, the sensitivity gradient of the blade's tip to the root is observable in the first three frequency orders in the x -direction. The tip is the most sensitive whereas the root is the least sensitive. Moreover, in the y -direction, the blade's two sides demonstrate a sensitive area, progressing from the allowances towards the middle. The sensitive zones, sub-sensitive zones, and non-sensitive zones occur in that order. Here are the extracted eigenvalues of each node for stiffness and mass sensitivity.

After obtaining the trend of sensitivity change at each node, finally, the first-order sensitivity values for the eigenvalues of titanium alloy thin-walled blades are calculated as follows.

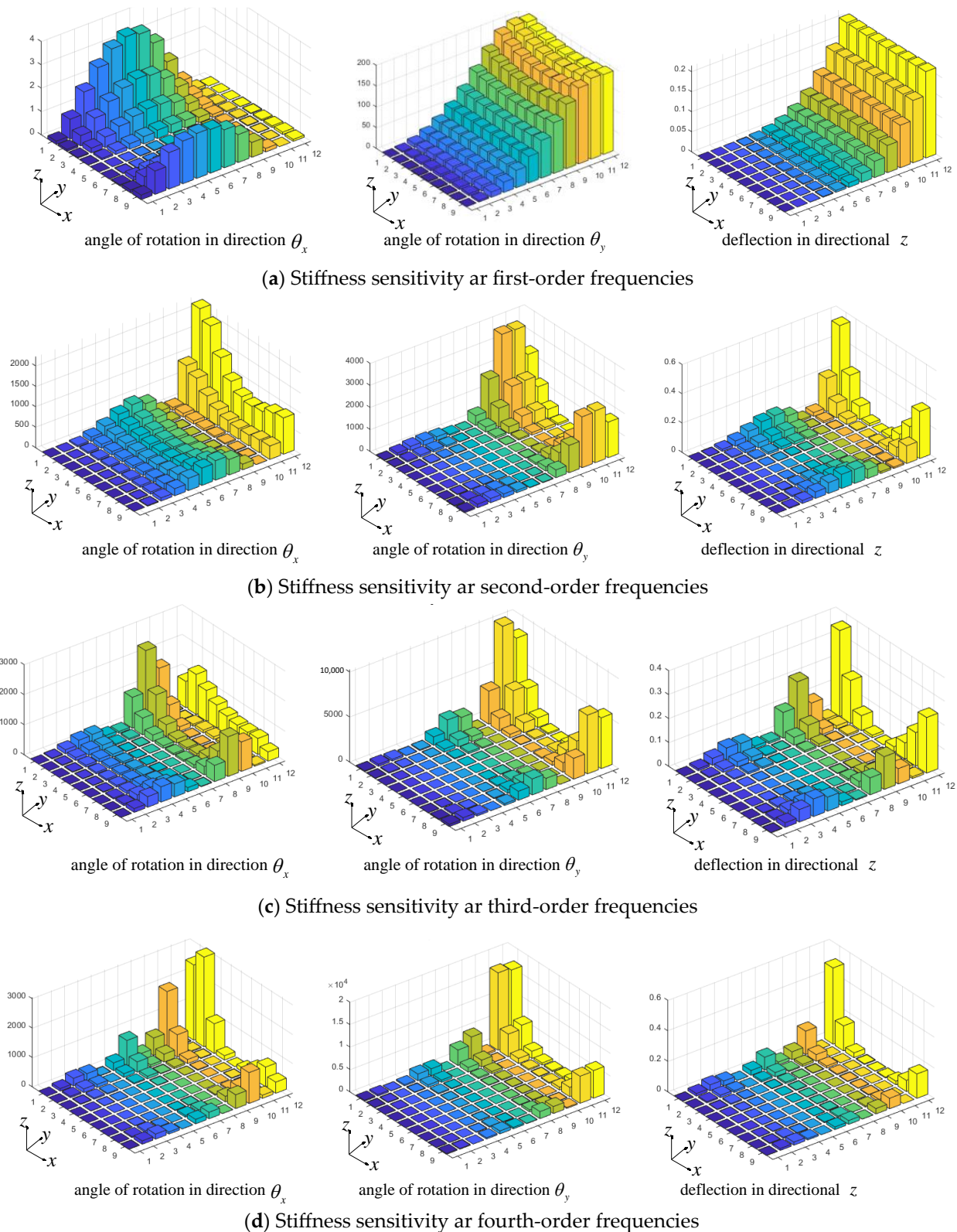
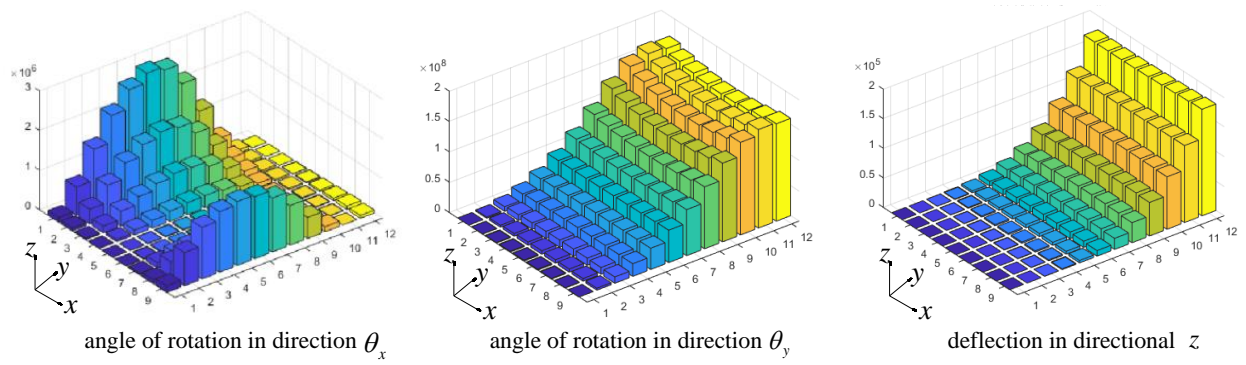
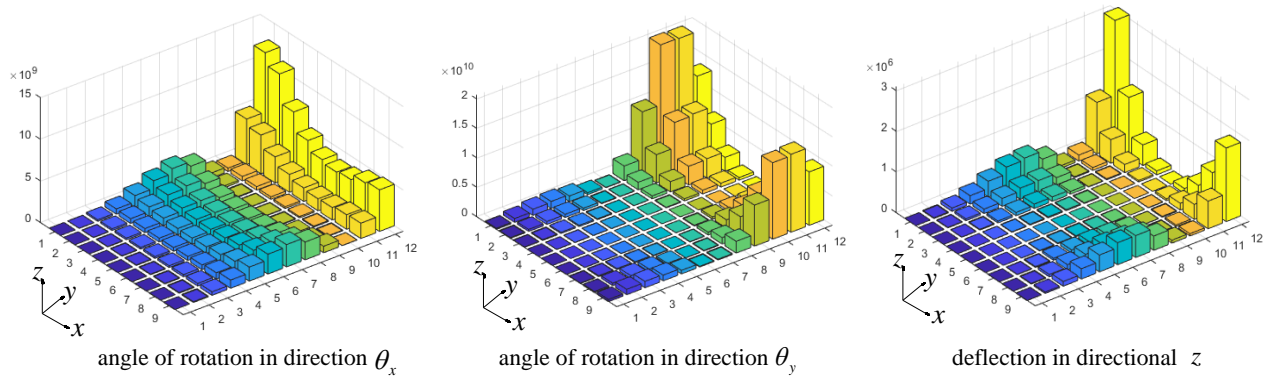


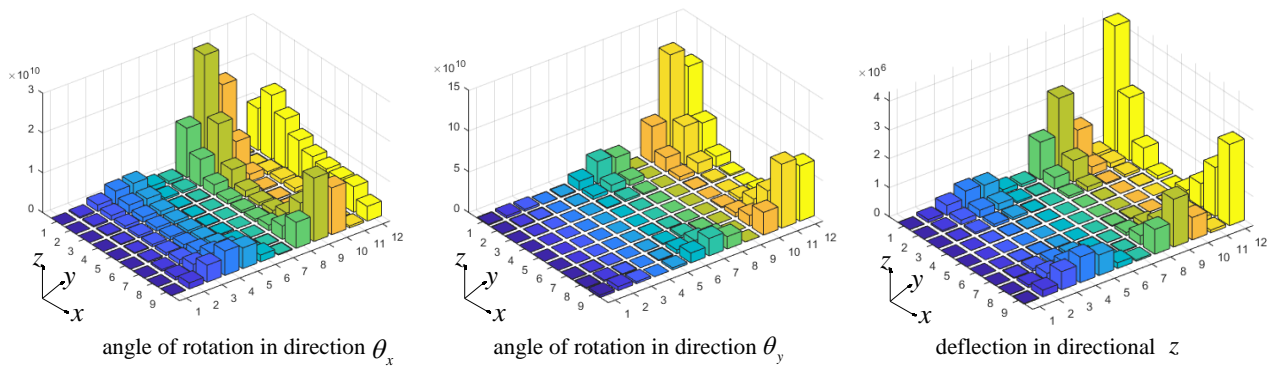
Figure 3. Calculation of eigenvalue sensitivity to stiffness.



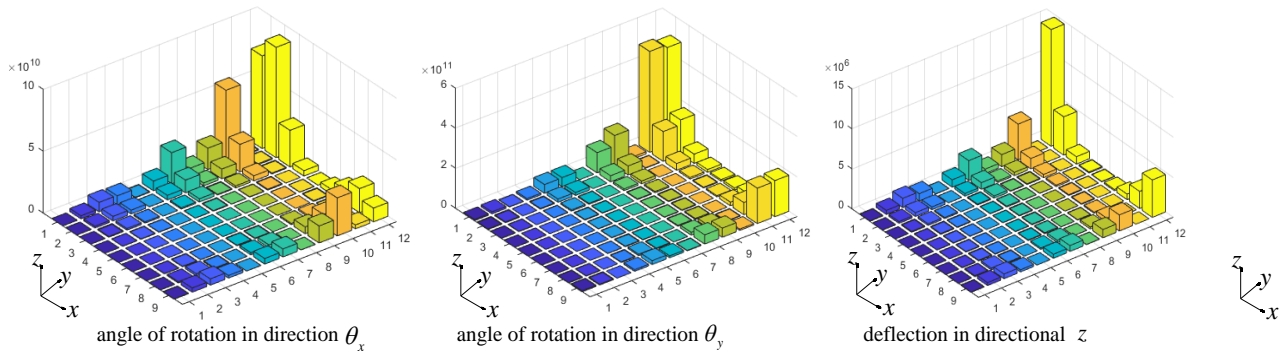
(a) Mass sensitivity at first-order frequencies



(b) Mass sensitivity at second-order frequencies



(c) Mass sensitivity at third-order frequencies



(d) Mass sensitivity at fourth-order frequencies

Figure 4. Calculation of eigenvalue sensitivity to mass.

$$\frac{\partial \lambda}{\partial k_{ij}} = \begin{bmatrix} -1.19 \times 10^{-7} & -2.55 \times 10^{-5} & -2.75 \times 10^{-4} & -1.26 \times 10^{-3} & -3.87 \times 10^{-3} & -0.94 \times 10^{-2} & -1.95 \times 10^{-2} & -3.65 \times 10^{-2} & -6.28 \times 10^{-2} & -1.01 \times 10^{-1} & -1.50 \times 10^{-1} & -2.10 \times 10^{-1} \\ -3.26 \times 10^{-6} & -7.84 \times 10^{-5} & -4.96 \times 10^{-4} & -1.81 \times 10^{-3} & -4.89 \times 10^{-3} & -1.10 \times 10^{-2} & -2.18 \times 10^{-2} & -3.92 \times 10^{-2} & -6.56 \times 10^{-2} & -1.02 \times 10^{-1} & -1.51 \times 10^{-1} & -2.10 \times 10^{-1} \\ -8.14 \times 10^{-6} & -1.34 \times 10^{-4} & -6.94 \times 10^{-4} & -2.26 \times 10^{-3} & -5.71 \times 10^{-3} & -1.23 \times 10^{-2} & -2.35 \times 10^{-2} & -4.13 \times 10^{-2} & -6.78 \times 10^{-2} & -1.04 \times 10^{-1} & -1.52 \times 10^{-1} & -2.10 \times 10^{-1} \\ -1.24 \times 10^{-5} & -1.77 \times 10^{-4} & -8.38 \times 10^{-4} & -2.58 \times 10^{-3} & -6.28 \times 10^{-3} & -1.32 \times 10^{-2} & -2.47 \times 10^{-2} & -4.28 \times 10^{-2} & -6.93 \times 10^{-2} & -1.06 \times 10^{-1} & -1.52 \times 10^{-1} & -2.10 \times 10^{-1} \\ -1.45 \times 10^{-5} & -1.98 \times 10^{-4} & -9.10 \times 10^{-4} & -2.74 \times 10^{-3} & -6.58 \times 10^{-3} & -1.36 \times 10^{-2} & -2.54 \times 10^{-2} & -4.37 \times 10^{-2} & -7.03 \times 10^{-2} & -1.07 \times 10^{-1} & -1.53 \times 10^{-1} & -2.10 \times 10^{-1} \\ -1.37 \times 10^{-5} & -1.92 \times 10^{-4} & -8.98 \times 10^{-4} & -2.73 \times 10^{-3} & -6.58 \times 10^{-3} & -1.37 \times 10^{-2} & -2.55 \times 10^{-2} & -4.39 \times 10^{-2} & -7.06 \times 10^{-2} & -1.07 \times 10^{-1} & -1.54 \times 10^{-1} & -2.11 \times 10^{-1} \\ -9.54 \times 10^{-6} & -1.57 \times 10^{-4} & -7.99 \times 10^{-4} & -2.54 \times 10^{-3} & -6.29 \times 10^{-3} & -1.33 \times 10^{-2} & -2.51 \times 10^{-2} & -4.35 \times 10^{-2} & -7.04 \times 10^{-2} & -1.07 \times 10^{-1} & -1.55 \times 10^{-1} & -2.12 \times 10^{-1} \\ -3.65 \times 10^{-6} & -9.94 \times 10^{-5} & -6.21 \times 10^{-4} & -2.18 \times 10^{-3} & -5.71 \times 10^{-3} & -1.25 \times 10^{-2} & -2.41 \times 10^{-2} & -4.24 \times 10^{-2} & -6.95 \times 10^{-2} & -1.07 \times 10^{-1} & -1.55 \times 10^{-1} & -2.14 \times 10^{-1} \\ -3.97 \times 10^{-8} & -3.56 \times 10^{-5} & -3.90 \times 10^{-4} & -1.69 \times 10^{-3} & -4.87 \times 10^{-3} & -1.12 \times 10^{-2} & -2.25 \times 10^{-2} & -4.07 \times 10^{-2} & -6.80 \times 10^{-2} & -1.06 \times 10^{-1} & -1.56 \times 10^{-1} & -2.16 \times 10^{-1} \end{bmatrix}$$

$$\frac{\partial \lambda}{\partial m_{ij}} = \begin{bmatrix} -9.98 \times 10^{-2} & -2.13 \times 10^1 & -2.30 \times 10^2 & -1.06 \times 10^3 & -3.23 \times 10^3 & -7.83 \times 10^3 & -1.63 \times 10^4 & -3.05 \times 10^4 & -5.25 \times 10^4 & -8.41 \times 10^4 & -1.26 \times 10^5 & -1.76 \times 10^5 \\ -2.72 \times 10^0 & -6.55 \times 10^1 & -4.16 \times 10^2 & -1.51 \times 10^3 & -4.09 \times 10^3 & -9.19 \times 10^3 & -1.83 \times 10^4 & -3.28 \times 10^4 & -5.48 \times 10^4 & -8.59 \times 10^4 & -1.26 \times 10^5 & -1.75 \times 10^5 \\ -6.80 \times 10^0 & -1.12 \times 10^2 & -5.80 \times 10^2 & -1.89 \times 10^3 & -4.77 \times 10^3 & -1.03 \times 10^4 & -1.97 \times 10^4 & -3.45 \times 10^4 & -5.66 \times 10^4 & -8.73 \times 10^4 & -1.27 \times 10^5 & -1.75 \times 10^5 \\ -1.03 \times 10^1 & -1.48 \times 10^2 & -7.00 \times 10^2 & -2.15 \times 10^3 & -5.25 \times 10^3 & -1.10 \times 10^4 & -2.07 \times 10^4 & -3.58 \times 10^4 & -5.79 \times 10^4 & -8.84 \times 10^4 & -1.28 \times 10^5 & -1.76 \times 10^5 \\ -1.2 \times 10^1 & -1.65 \times 10^2 & -7.60 \times 10^2 & -2.29 \times 10^3 & -5.49 \times 10^3 & -1.14 \times 10^4 & -2.12 \times 10^4 & -3.65 \times 10^4 & -5.87 \times 10^4 & -8.92 \times 10^4 & -1.28 \times 10^5 & -1.76 \times 10^5 \\ -1.14 \times 10^1 & -1.61 \times 10^2 & -7.50 \times 10^2 & -2.28 \times 10^3 & -5.50 \times 10^3 & -1.14 \times 10^4 & -2.13 \times 10^4 & -3.67 \times 10^4 & -5.90 \times 10^4 & -8.97 \times 10^4 & -1.29 \times 10^5 & -1.77 \times 10^5 \\ -7.94 \times 10^0 & -1.31 \times 10^2 & -6.67 \times 10^2 & -2.12 \times 10^3 & -5.26 \times 10^3 & -1.11 \times 10^4 & -2.10 \times 10^4 & -3.64 \times 10^4 & -5.88 \times 10^4 & -8.98 \times 10^4 & -1.30 \times 10^5 & -1.78 \times 10^5 \\ -3.05 \times 10^0 & -8.30 \times 10^1 & -5.19 \times 10^2 & -1.82 \times 10^3 & -4.77 \times 10^3 & -1.04 \times 10^4 & -2.01 \times 10^4 & -3.55 \times 10^4 & -5.81 \times 10^4 & -8.95 \times 10^4 & -1.30 \times 10^5 & -1.79 \times 10^5 \\ -3.32 \times 10^{-2} & -2.98 \times 10^1 & -3.26 \times 10^2 & -1.41 \times 10^3 & -4.07 \times 10^3 & -9.40 \times 10^3 & -1.88 \times 10^4 & -3.40 \times 10^4 & -5.68 \times 10^4 & -8.88 \times 10^4 & -1.30 \times 10^5 & -1.80 \times 10^5 \end{bmatrix}$$

3.2. Non-Uniform Allowance Distribution of Titanium Alloy Thin-Walled Blade Finishing

Under the condition of obtaining the sensitivity and setting the eigenvalue level constraints, such as taking the mean sensitivity of the blade as the level reference value, the amount of change in the thickness t of the grid cells can be calculated based on the non-uniform allowance design steps (3–5) in the finishing stage. The value of the thickness t is obtained by calculation and measurement as follows.

$$t_{ij} = \begin{bmatrix} 0.664489 & 1.598100 & 2.709500 & 3.371400 & 3.645500 & 3.561500 & 3.125800 & 2.323200 & 1.112600 \\ 0.528346 & 1.549600 & 2.802300 & 3.566800 & 3.822000 & 3.612200 & 3.019100 & 2.130200 & 0.998928 \\ 0.612617 & 1.563900 & 2.767200 & 3.513000 & 3.738900 & 3.480900 & 2.846700 & 1.957200 & 0.907683 \\ 0.675002 & 1.577300 & 2.637900 & 3.297800 & 3.488400 & 3.231700 & 2.630300 & 1.796400 & 0.831464 \\ 0.705875 & 1.537800 & 2.445000 & 3.009100 & 3.168500 & 2.936400 & 2.397900 & 1.643100 & 0.761881 \\ 0.686540 & 1.460400 & 2.254700 & 2.742800 & 2.875200 & 2.660800 & 2.173500 & 1.490500 & 0.691834 \\ 0.647066 & 1.373300 & 2.082300 & 2.512400 & 2.618100 & 2.409500 & 1.957200 & 1.336800 & 0.623313 \\ 0.598048 & 1.267600 & 1.888000 & 2.258000 & 2.339700 & 2.144200 & 1.737100 & 1.187200 & 0.562848 \\ 0.541569 & 1.146700 & 1.677800 & 1.988500 & 2.050700 & 1.876500 & 1.523000 & 1.047900 & 0.510375 \\ 0.484355 & 1.023600 & 1.473000 & 1.732200 & 1.780800 & 1.630400 & 1.329200 & 0.924291 & 0.465330 \\ 0.436785 & 0.913686 & 1.295500 & 1.516000 & 1.556900 & 1.427500 & 1.169100 & 0.821592 & 0.427293 \\ 0.393285 & 0.830623 & 1.163100 & 1.356400 & 1.393400 & 1.280200 & 1.052200 & 0.745560 & 0.397133 \\ 0.370252 & 0.784887 & 1.091300 & 1.267100 & 1.301900 & 1.198200 & 0.986841 & 0.701145 & 0.374390 \end{bmatrix}$$

Next, the model simplification in Figure 5a is carried out, and then the 2D cross-section shape meshing is shown in Figure 5b. Here, with the standard grid cell (5 mm × 5 mm), the calculation can be obtained due to the simplification and the shape of the blade body surface itself, the formation of a series of irregular grid cells, along the longitudinal direction of the blade body, the length of 5 mm, and the width of the following order, 3.4365 mm, 3.6309 mm, 3.7157 mm, 3.7582 mm, 3.8133 mm, 3.9092 mm, 4.0327 mm, 4.1640 mm, 4.3027 mm, 4.4499 mm, 4.6040 mm, 4.7625 mm, and 4.9228 mm. Finally, according to the mesh node thickness subdivided, the coordinates of the interpolation point of the intermediate part of each cross-section can be obtained to construct the cross-section curves, as shown in Figure 5c.

Finally, only the amount of height change of the grid cells at the three key sections is extracted, and first the cross-section curve of the blade performs the smooth processing is constructed as shown in Figure 6a. Then, the surface reconstruction through the mesh surface is performed, the surface of the allowances distribution in the finishing stage is obtained, and the whole design process is as shown in Figure 6b. The blade body is cut based on the actual blade. Lastly, the non-uniform allowance bias surface in the finishing stage can be further used as the driving surface for finishing programming to form a helical wrap-around tool position trajectory as shown in Figure 6c.

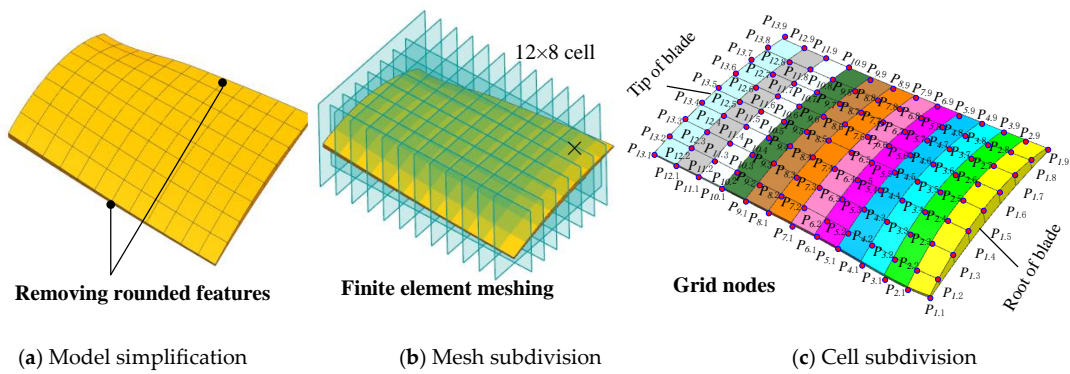
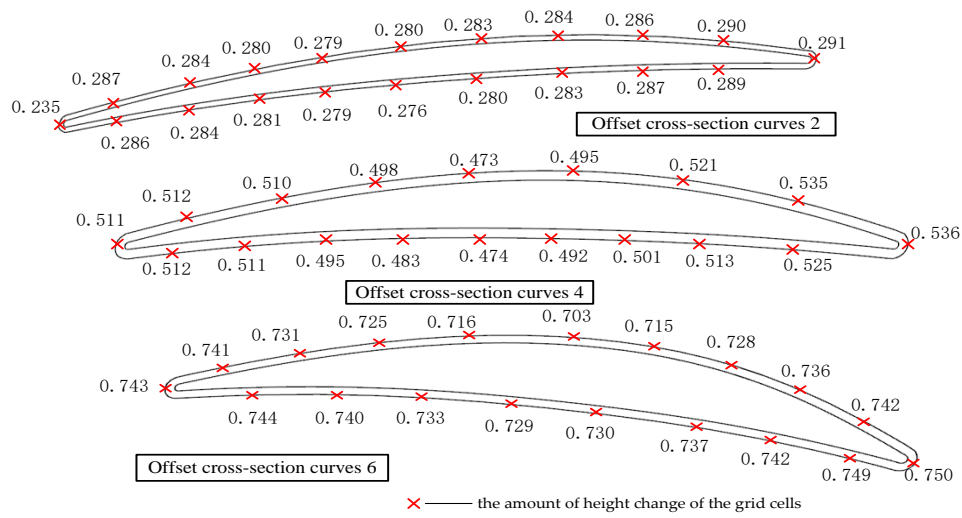
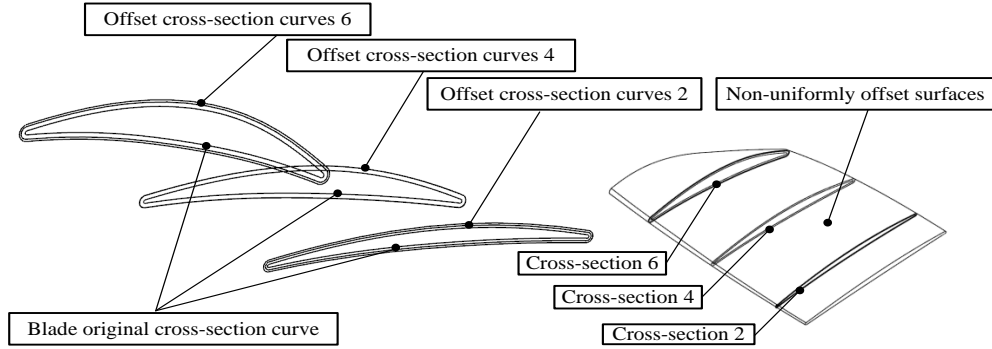


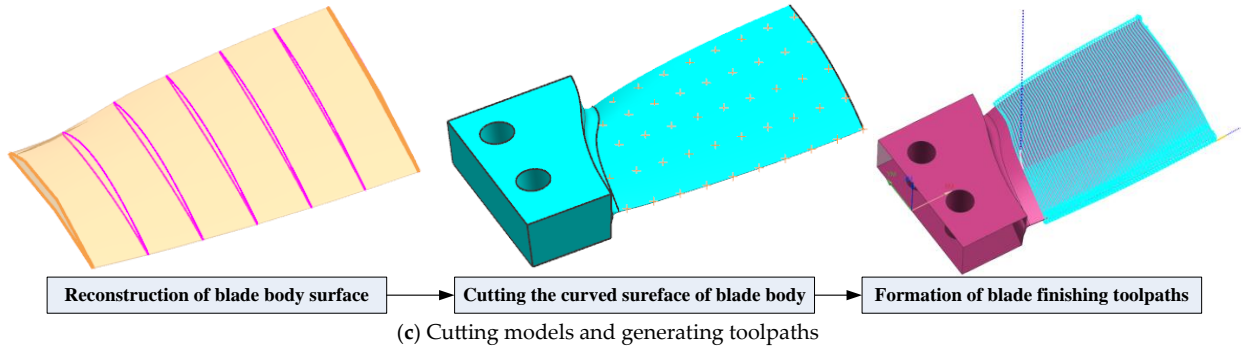
Figure 5. Mesh cell subdivision of the blade.



(a) Construction of cross-sectional interpolation points



(b) Construction of the biased surface



(c) Cutting models and generating toolpaths

Figure 6. Finish design with non-uniform allowances distribution.

3.3. Experimental Verification of Thin-Walled Blade Milling

In order to simulate actual blade operating conditions, the base of a single blade is clamped in a flat nose pliers along the length direction, similar to a mortise and tenon structure. Place the blades in a free state. The stability state of cutting is directly reflected through the acceleration spectrum during the cutting process. The vibration testing principle in milling is depicted as in Figure 7. The ECON-AVANT-MI-7008 data acquisition and analyzer from Hangzhou Yiheng Technology Co. (Hangzhou, China) are utilized, alongside the Dytran3032A acceleration sensor for accuracy and reliability of measurement and data analysis. To monitor vibration amplitude during milling, the acceleration sensor was affixed to the tip position of the blade and acquired the dynamic acceleration signal in real-time via zoning. Prior to measurement, it is essential to calibrate the phase characteristics of the measurement channel for force and vibration acceleration signals to avoid any phase differences which could lead to measurement errors. Roughness was measured using a TR100 Roughness Meter manufactured by Beijing Times Yuanfeng Technology Co. (Beijing, China) Surface roughness was evaluated using Ra as the index, with testing conducted in the feeding direction. Each experiment was conducted in groups of five, with the average value taken as the final result. The experimental test site is illustrated in Figure 8.

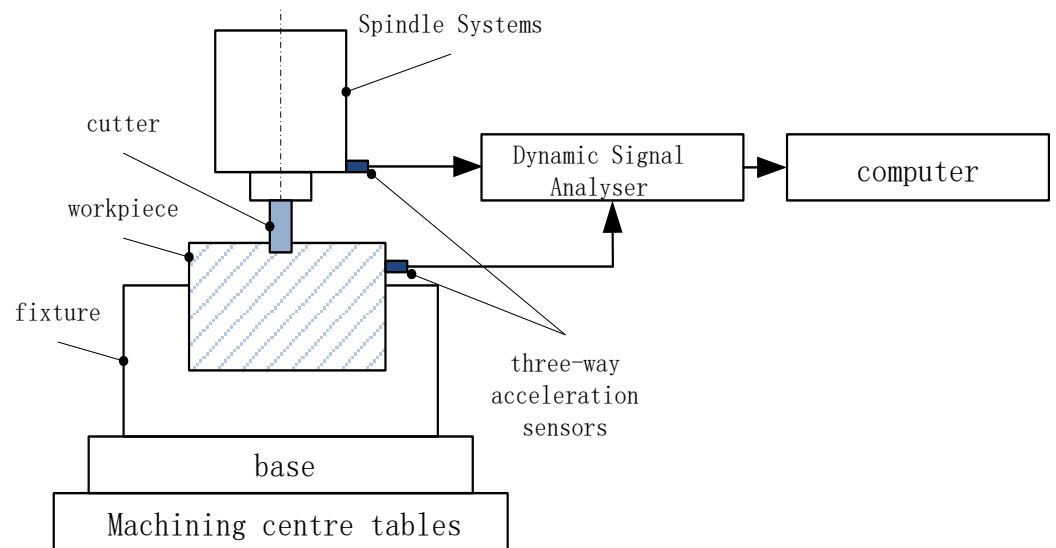
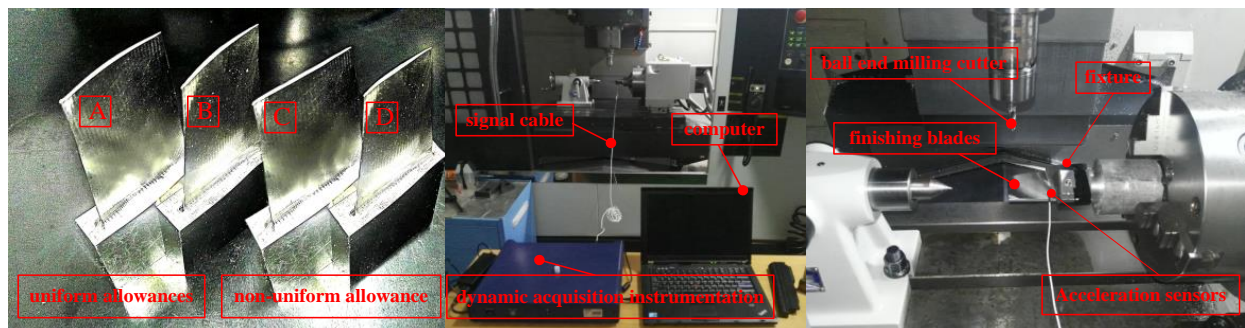


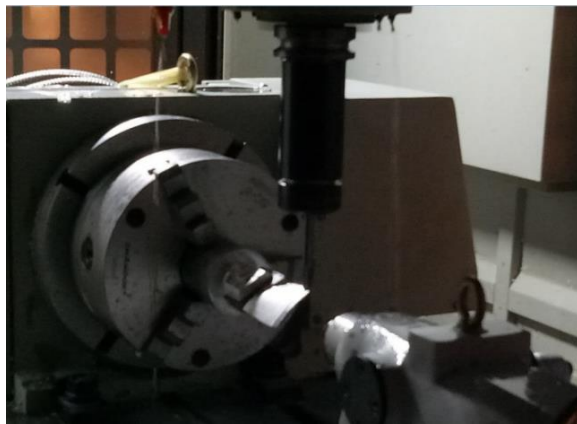
Figure 7. Schematic diagram of milling vibration test.



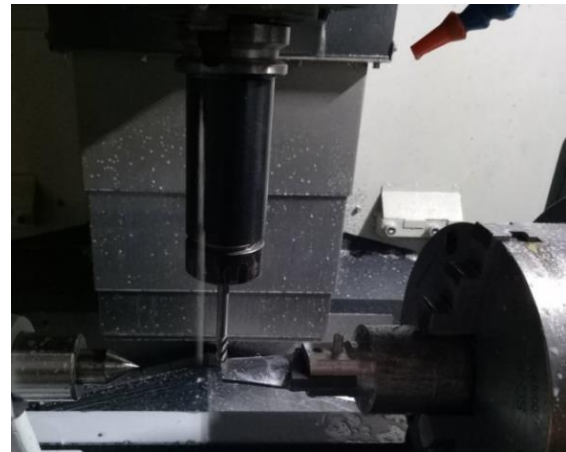
(a) Design of allowances distribution

(b) Acceleration spectrum acquisition

Figure 8. Cont.



(c) Milling processing site of blade basin



(d) Milling processing site of blade suction

Figure 8. Blade milling machining test site.

To ensure the proposed method's reliability in the finishing stage, a traditional uniform allowance distribution structure design was shown as A and B in Figure 8a, alongside the non-uniform allowance structure design shown as C and D in Figure 8a, with a guarantee of the same amount of removal volume. The vibration acceleration spectrum acquired during cutting is shown in Figure 8b. The experiments were conducted using a VMP-850A four-axis vertical machining center equipped with a BT40 spindle and toolholder, a carbide ball end milling cutter with a diameter of 8 mm and a tool overhang of $L = 30$ mm. The axial depth of cut was $a_p = 0.2$ mm, and the cutting speed was $f = 1100$ mm/min with a milling mode of down milling and a blade material of TC4 titanium alloy. The blade basin milling process is shown in Figure 8c. The blade suction milling process is shown in Figure 8d. The cutting tool was cooled with emulsion.

3.4. Results and Discussion

(1) Vibration acceleration spectrum analysis

The acceleration spectra of the blade basin and suction tip parts are collected as shown in Figure 9, and it can be seen from the vibration acceleration spectra at the milled tip parts that when using the processing strategy of non-uniform stiffness enhancement proposed herein, both the value of the peak acceleration and the density of the acceleration spectra along the distribution of the vibration frequency are much smaller than those with uniform allowance milling process.

(2) Machining surface topography analysis

The surface morphology after machining of the two process strategies is shown in Figure 10, and the vibration pattern on the surface of the blade basin e.g., Figure 10a—A surface and blade suction e.g., Figure 10a—B surface is very significant when using the traditional process strategy of uniform allowance milling. However, the non-uniform allowance milling using the process strategy proposed herein significantly reduces the vibration pattern regardless of the blade basin e.g., Figure 10b—A surface and blade suction e.g., Figure 10b—B surface. The results are consistent when testing the roughness of both process schemes. Specimen A adopts the traditional uniform allowance program for the surface geometric accuracy testing blade basin and suction, the geometric cross-section part of the super poor, the surface of the existence of obvious vibration pattern, and the tip part of the blade is particularly significant. The root part of the blade vibration marks will be shallow. The measurement of the sampling part of the roughness of the suction R_a is about $2.77 \mu\text{m}$ and the basin R_a $2.68 \mu\text{m}$. Specimen B adopts the non-uniform process strategy for the surface geometric accuracy testing of the blade basin and suction. The strategy can ensure the size as well as the smooth cross-section of the blade body profile transition. It

also guarantees obvious vibration pattern, with the sampling part roughness the suction Ra measured about 1.85 μm and the basin Ra 1.73 μm .

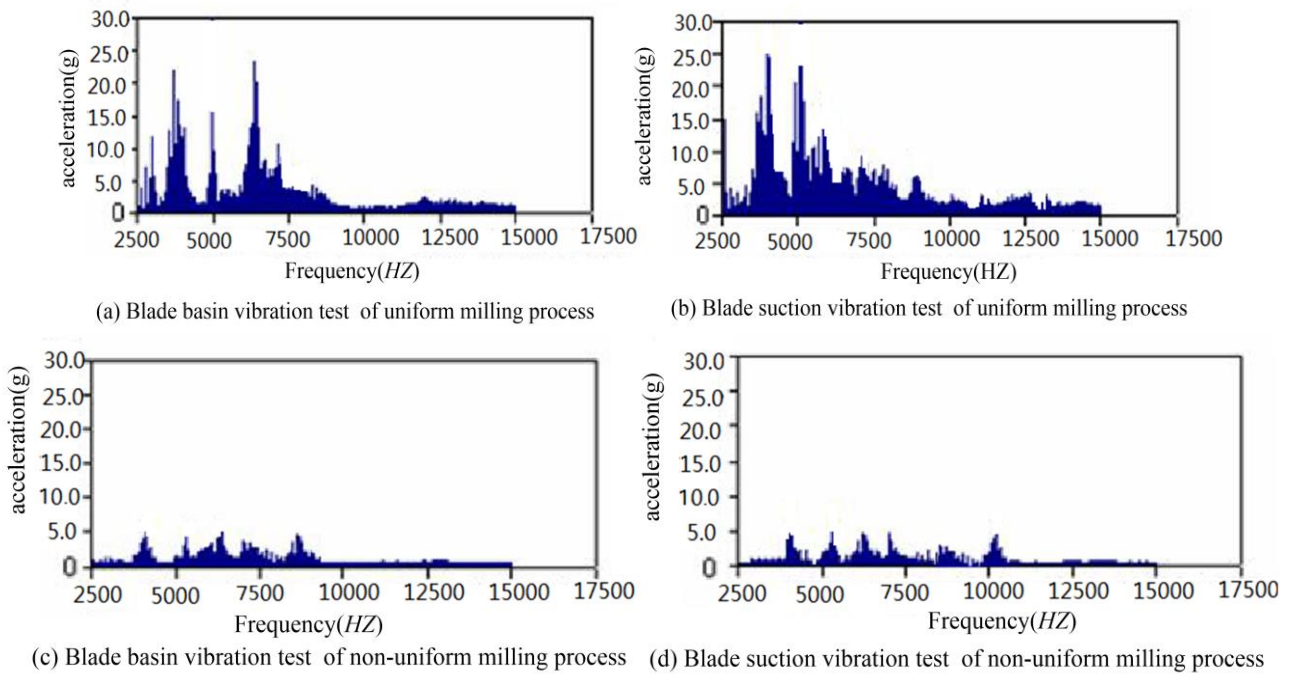


Figure 9. Comparison of acceleration spectra for milling process options.

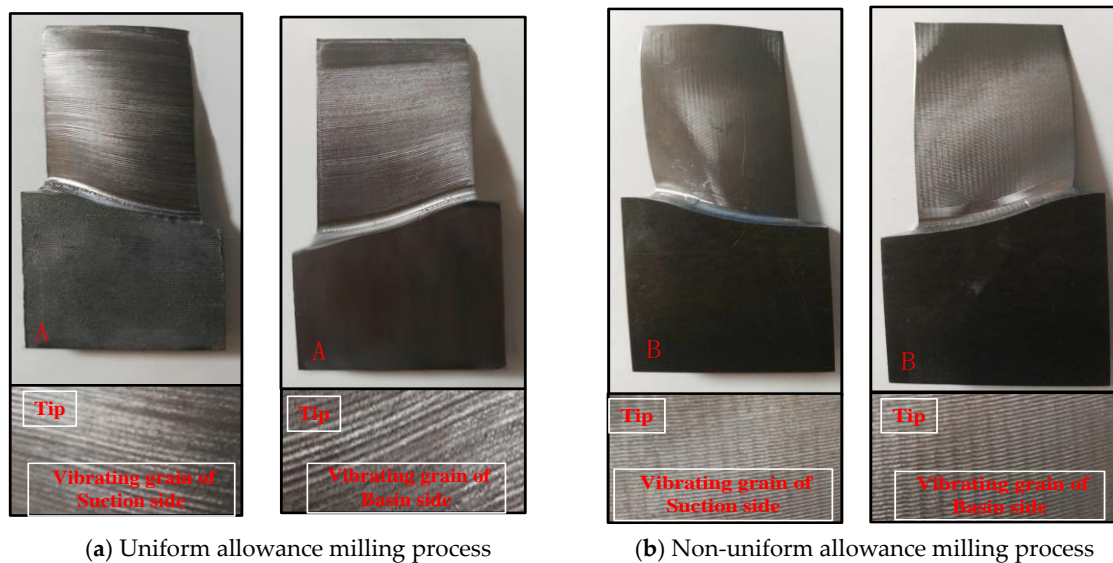


Figure 10. Comparison of surface morphology between two milling process.

In fact, some scholars have already done a lot of basic work on improving the rigidity of the workpiece itself through non-uniform allowance. Reference [36] facing complex thin-walled blade parts, based on the theory of regenerative vibration analysis, established a comparison chart of the stability lobe of uniform allowance and non-uniform allowance. Theoretically, it shows that non-uniform allowance is beneficial to improve the milling stability of the blade and reduce the cutting vibration of the blade during the cutting process. However, in the design of the allowance, a rough gradient layout based on experience is adopted, which limits the accuracy of the allowance distribution. Reference [39] proposed a non-uniform allowance allocation method based interim state stiffness of thin-walled parts finishing machining features. The stiffness index is simplified as proportional to the

area and thickness of the machined surface. By evaluating the interim state stiffness of each machining feature and allocating non-uniform allowances, the stiffness in finishing machining of thin-walled parts is ensured. This method, similar to the former, is also an empirical allowance non-uniform design, which can be well approximated for thin-walled frame parts with geometric structural rules. However, this method is not suitable for complex composite features like blades. Reference [36] proposes a non-uniform allowance planning method for thin-walled parts based on static deformation constraints of the workpiece. This method calculates the relative deformation of the tool contact point based on a steady-state cutting force numerical simulation model, increases the thickness of the node material in reverse to improve stiffness, and finally obtains the distribution surface of finishing machining allowance through smooth fitting face. Reference [37], compared to reference [36], is also based on the idea of static deformation. A mathematical model for predicting the deformation of thin-walled parts during milling based on the Rayleigh Ritz method was established. The thin-walled parts were discretized to solve the unit allowance volume, and the non-uniform allowance design of the workpiece was completed through smoothing. This method has improved computational efficiency and is relatively simple compared to the former. However, due to the influence of deformation prediction accuracy, and secondly, the topological structure characteristics of the part structure have not been taken into account, there are still certain limitations in the application of thin-walled complex structural components. Reference [38] proposes to measure the static deformation of parts on the machine, then calculate the allowance compensation value, and achieve stable milling of thin-walled parts by adaptively adjusting the cutting depth during precision machining. This method is intuitive, simple, and effective, but it is limited by in-machine measurement and first part trial cutting and is currently only suitable for conventional thin-walled components such as partition frames and wall panels.

This paper is based on the finite element method and proposes a stiffness sensitivity theory to enhance the process stiffness through the subdivision of finite element mesh. From the experimental verification analysis and comparison in this section, it can be seen that, on the one hand, it can fit complex structural components well, and, on the other hand, numerical calculations can accurately design the allowance. Compared with previous work, this method has a certain degree of generalizability and adaptability.

4. Conclusions

Targeting the issue of chatter in finishing thin-walled aerospace blade, the proposed process optimizes a non-uniform allowance using the sensitivity to process stiffness for improved surface quality control. The machining chatter of thin-walled parts can be mitigated to a great extent, resulting in a reduction of cutting force fluctuations and vibration. This leads to an improvement of surface roughness of the parts and guarantees a smooth cutting process of thin-walled blades. Therefore, the aforementioned findings infer that the milling process of thin-walled parts can be enhanced. The following conclusions can be drawn.

(1) The non-uniform allowance structure layout demonstrates favorable qualities for achieving a stable state in the cutting process. This is evidenced by the acquisition process of the dynamic acceleration spectrum. The convergence towards a stable state indicates the effectiveness of the non-uniform allowance distribution.

(2) The implementation of the non-uniform allowance process method leads to a significant increase in the natural frequency, approximately 100 Hz. This increase indirectly reflects an improvement in the workpiece process stiffness. Moreover, the overall frequency exhibits an upward trend while the vibration amplitude decreases.

(3) An analysis of the processing surface morphology reveals that the non-uniform allowance process generates superior surface quality compared to uniform transition methods. The resulting surface exhibits smoother morphology, devoid of significant vibration patterns. Additionally, the non-uniform allowance process contributes to a reduction in roughness by nearly 35%.

The method proposed in this paper through the non-uniform allowance distribution compared with the previous workers has the characteristics of more accurate allowance distribution, more convenient calculation, can be combined with numerical algorithms to quickly achieve the design of edge distribution, without the need for finite element software simulation. Therefore, it has a certain reference significance in actual engineering.

Author Contributions: Y.L.: Methodology, investigation, formal analysis and draft writing. W.T.: Project administration, formal analysis, review, and editing. J.Z.: Project administration, formal analysis, review, and editing. F.D.: Supervision, project administration, and review. All authors have read and agreed to the published version of the manuscript.

Funding: This work is supported by the National Natural Science Foundation of China (Grant No. 52075451), the Natural Science Basic Research Program of Shaanxi (Program No. 2023-JC-YB-347), the Aeronautical Science Foundation of China (Grant No. 2019ZE053008).

Data Availability Statement: All data and materials used or analyzed during the current study are included in this manuscript.

Conflicts of Interest: The authors declare no conflict of interest.

References

1. Tian, W.J.; Ren, J.X.; Zhou, J.H.; Wang, D.Z. Dynamic modal prediction and experimental study of thin-walled workpiece removal based on perturbation method. *Int. J. Adv. Manuf. Technol.* **2018**, *94*, 2099–2113. [\[CrossRef\]](#)
2. Zhang, Z.X.; Zhang, Z.; Zhang, D.H.; Luo, M. Milling distortion prediction for thin-walled component based on the average MIRS in specimen machining. *Int. J. Adv. Manuf. Technol.* **2020**, *111*, 3379–3392. [\[CrossRef\]](#)
3. Wang, D.Z.; Ren, J.X.; Tian, W.J.; Shi, K.N.; Zhang, B.G. Predicting the dynamics of thin-walled parts with curved surfaces in milling based on FEM and Taylor series. *Int. J. Adv. Manuf. Technol.* **2019**, *103*, 927–942. [\[CrossRef\]](#)
4. Xiang, J.F.; Yi, J. Deformation mechanism in wax supported milling of thin-walled structures based on milling forces stability. *CIRP J. Manuf. Sci. Technol.* **2021**, *32*, 356–369. [\[CrossRef\]](#)
5. Li, J.B.; Zhang, D.H.; Wu, B.H.; Liu, W.W. Study on design and optimization of clamping scheme in NC machining of thin-walled blades. *China Mech. Eng.* **2012**, *23*, 1341–1344, 1349.
6. Wang, X.J.; Song, Q.H.; Liu, Z.Q. Position-dependent stability prediction for multi-axis milling of the thin-walled component with a curved surface. *Appl. Sci.* **2020**, *10*, 8779. [\[CrossRef\]](#)
7. Cong, J.M.; Mo, R.; Zhang, Y.; Wang, Q. Iterative Learning Modeling Method of Error Compensation for Machining of Aeroengine Thin-wall Blade. *Mech. Sci. Technol. Aerosp. Eng.* **2019**, *38*, 73–79.
8. Ma, J.J.; Li, Y.F.; Zhang, D.H.; Zhao, B.; Wang, G.; Pang, X.Y. Dynamic response prediction model of thin-wall workpiece–fixture system with magnetorheological damping in milling. *J. Manuf. Process.* **2022**, *74*, 500–510. [\[CrossRef\]](#)
9. Hou, Y.H.; Zhang, D.H.; Mei, J.W.; Zhang, Y.; Luo, M. Geometric modelling of thin-walled blade based on compensation method of machining error and design intent. *J. Manuf. Process.* **2019**, *44*, 327–336. [\[CrossRef\]](#)
10. Yao, C.F.; Zhang, J.Y.; Cui, M.C.; Tan, L.; Shen, X.H. Machining deformation prediction of large fan blades based on loading uneven allowances stress. *Int. J. Adv. Manuf. Technol.* **2020**, *107*, 4345–4356. [\[CrossRef\]](#)
11. Hamann, D.; Eberhard, P. Stability analysis of milling processes with varying workpiece dynamics. *Multibody Syst. Dyn.* **2018**, *42*, 383–396. [\[CrossRef\]](#)
12. Wan, M.; Ma, Y.C.; Zhang, W.H.; Yang, Y. Study on the construction mechanism of stability lobes in milling process with multiple modes. *Int. J. Adv. Manuf. Technol.* **2015**, *79*, 589–603. [\[CrossRef\]](#)
13. Wang, L.P.; Li, W.T.; Yu, G. Time domain study on the construction mechanism of milling stability lobe diagrams with multiple modes. *J. Manuf. Sci. Eng.* **2022**, *144*, 021007. [\[CrossRef\]](#)
14. Yang, J.Z.; Li, J.W.; Qu, W.X.; Zhang, D.; Zhou, J.Q. Analysis of Milling Process Stability. *China Mech. Eng.* **2013**, *24*, 360–365.
15. Li, Z.Y.; Sun, Y.W.; Guo, D.M. Chatter prediction utilizing stability lobes with process damping in finish milling of titanium alloy thin-walled workpiece. *Int. J. Adv. Manuf. Technol.* **2017**, *89*, 2663–2674. [\[CrossRef\]](#)
16. Liu, Y.; Li, T.X.; Liu, K.; Zhang, Y.M. Chatter reliability prediction of turning process system with uncertainties. *Mech. Syst. Signal Process.* **2016**, *66–67*, 232–247. [\[CrossRef\]](#)
17. Liu, Y.; Meng, L.L.; Liu, K.; Zhang, Y.M. Chatter reliability of milling system based on first-order second-moment method. *Int. J. Adv. Manuf. Technol.* **2016**, *87*, 801–809. [\[CrossRef\]](#)
18. Zhan, D.N.; Jiang, S.L.; Li, S.K.; Sun, Y.W. A hybrid multi-step method based on 1/3 and 3/8 Simpson formulas for milling stability prediction. *Int. J. Adv. Manuf. Technol.* **2022**, *120*, 265–277. [\[CrossRef\]](#)
19. Huang, X.Z.; Zhang, Y.M.; Lv, C.M. Probabilistic analysis of dynamic stability for milling process. *Nonlinear Dyn.* **2016**, *86*, 2105–2114. [\[CrossRef\]](#)
20. Hu, S.; Huang, X.Z.; Zhang, Y.M.; Lv, C.M. Reliability analysis of the chatter stability during milling using a neural network. *Int. J. Aerosp. Eng.* **2016**, *2016*, 5259821. [\[CrossRef\]](#)

21. Zhang, N.; Shi, Y.Y.; Chen, Z.; Chen, H.X.; Liu, J.; Zhao, P. Chatter reliability prediction of side milling blisk. *Xibei Gongye Daxue Xuebao/J. Northwestern Polytech. Univ.* **2021**, *39*, 111–118. [[CrossRef](#)]
22. Li, X.H.; Wan, S.K.; Yuan, J.P.; Yin, Y.J.; Hong, J. Active suppression of milling chatter with LMI-based robust controller and electromagnetic actuator. *J. Mater. Process. Technol.* **2021**, *297*, 117238. [[CrossRef](#)]
23. Chen, P.W.; Zhai, J.; Zhang, X.M.; Zhang, H.T.; Ding, H. Research on Active Vibration Control of Thin-Walled Workpiece in Milling Based on Voice Coil Motor. In Proceedings of the Intelligent Robotics and Applications: 6th International Conference, ICIRA 2013, Busan, Republic of Korea, 25–28 September 2013; Springer: Berlin/Heidelberg, Germany, 2013; pp. 503–512.
24. Du, J.A.; Long, X.H. Chatter suppression for milling of thin-walled workpieces based on active modal control. *J. Manuf. Process.* **2022**, *84*, 1042–1053. [[CrossRef](#)]
25. Buransky, I.; Bracik, M.; Simna, V.; Vopat, T. Influence of end mill variable pitch on surface quality of aluminium thin-walled parts. *MM Sci. J.* **2018**, 2552–2557. [[CrossRef](#)]
26. Tehranizadeh, F.; Berenji, K.R.; Yildiz, S.; Budak, E. Chatter stability of thin-walled part machining using special end mills. *CIRP Ann.* **2022**, *71*, 365–368. [[CrossRef](#)]
27. Zheng, M.L.; Liu, Y.X.; Nie, W.Y.; Xu, S.C.; Bi, Y.Q. Vibration response analysis of thin-walled workpiece considering material removal effects during machining with variable pitch end mill. *Int. J. Adv. Manuf. Technol.* **2022**, *123*, 1607–1623. [[CrossRef](#)]
28. Guo, Q.; Jiang, Y.; Zhao, B.; Ming, P.M. Chatter modeling and stability lobes predicting for non-uniform helix tools. *Int. J. Adv. Manuf. Technol.* **2016**, *87*, 251–266. [[CrossRef](#)]
29. Jiang, S.L.; Zhan, D.N.; Liu, Y.; Sun, Y.W.; Xu, J.T. Modeling of variable-pitch/helix milling system considering axially varying dynamics with cutter runout offset and tilt effects. *Mech. Syst. Signal Process.* **2022**, *168*, 108674. [[CrossRef](#)]
30. Wu, Y.; Wang, K.; Zheng, G.; Lv, B.; He, Y. Experimental and simulation study on chatter stability region of integral impeller with non-uniform allowance. *Sci. Prog.* **2020**, *103*, 0036850420933418. [[CrossRef](#)]
31. Tian, W.J.; Ren, J.X.; Wang, D.Z.; Zhang, B.G. Optimization of non-uniform allowance process of thin-walled parts based on eigenvalue sensitivity. *Int. J. Adv. Manuf. Technol.* **2018**, *96*, 2101–2116. [[CrossRef](#)]
32. Jiang, X.H.; Wu, K.; Zhang, Y.; He, S.R. Improved vibration suppression modeling for reinforcement clamping by eco-friendly magnetorheological fluid during milling of annular thin-walled workpiece. *Int. J. Precis. Eng. Manuf.-Green Technol.* **2022**, *9*, 1511–1526. [[CrossRef](#)]
33. Yuan, X.; Wang, S.T.; Mao, X.Y.; Liu, H.Q.; Liang, Z.S.; Guo, Q.S.; Yan, R. Forced vibration mechanism and suppression method for thin-walled workpiece milling. *Int. J. Mech. Sci.* **2022**, *230*, 107553. [[CrossRef](#)]
34. Dang, X.B.; Wan, M.; Zhang, W.H.; Yang, Y. Chatter analysis and mitigation of milling of the pocket-shaped thin-walled workpieces with viscous fluid. *Int. J. Mech. Sci.* **2021**, *194*, 106214. [[CrossRef](#)]
35. Zhang, Z.; Li, H.G.; Liu, X.B.; Zhang, W.Y.; Meng, G. Chatter mitigation for the milling of thin-walled workpiece. *Int. J. Mech. Sci.* **2018**, *138–139*, 262–271. [[CrossRef](#)]
36. Zhang, Z.Z.; Cai, Y.L.; Xi, X.L.; Wang, H.T. Non-uniform machining allowance planning method of thin-walled parts based on the workpiece deformation constraint. *Int. J. Adv. Manuf. Technol.* **2023**, *124*, 2185–2198. [[CrossRef](#)]
37. Li, X.; Yuan, J.T.; Wang, Z.H.; Zhang, B. Study on Deformation Control of Thin-walled Titanium Alloy Parts in Non-uniform Allowance Machining Based on Rayleigh-Ritz Method. *China Mech. Eng.* **2020**, *31*, 1378–1385.
38. Jiang, S.; Li, Y.G.; Liu, C.Q. A non-uniform allowance allocation method based on interim state stiffness of machining features for NC programming of structural parts. *Vis. Comput. Ind. Biomed. Art* **2018**, *1*, 4. [[CrossRef](#)]
39. Wang, G.; Li, W.L.; Tong, G.; Pang, C.T. Improving the machining accuracy of thin-walled parts by online measuring and allowance compensation. *Int. J. Adv. Manuf. Technol.* **2017**, *92*, 2755–2763. [[CrossRef](#)]

Disclaimer/Publisher’s Note: The statements, opinions and data contained in all publications are solely those of the individual author(s) and contributor(s) and not of MDPI and/or the editor(s). MDPI and/or the editor(s) disclaim responsibility for any injury to people or property resulting from any ideas, methods, instructions or products referred to in the content.